Materials Transactions, Vol. 49, No. 4 (2008) pp. 805 to 811

Active Hydroxyl Groups on Surface Oxide Film of Titanium, 316L Stainless Steel, and Cobalt-Chromium-Molybdenum Alloy and Its Effect on the Immobilization of Poly(Ethylene Glycol)

Yuta Tanaka[1,*1], Haruka Saito[2,*1], Yusuke Tsutsumi[1,*2], Hisashi Doi[1], Hachiro Imai[2] and Takao Hanawa[1]

[1]*Institute of Biomaterials and Engineering, Tokyo Medical and Dental University, Tokyo 101-0062, Japan*
[2]*Department of Materials Science, Shibaura Institute of Technology, Tokyo 135-8548, Japan*

The concentrations of hydroxyl groups located inside and on the surface oxide films of a commercially pure titanium, cp-Ti, a type 316L austenitic stainless steel, SS, and a cobalt-chromium-molybdenum alloy, Co-Cr-Mo, were evaluated using X-ray photoelectron spectroscopy, XPS, and a zinc-complex substitution technique. As a result, the concentrations of the hydroxyl groups detected by the zinc-complex substitution technique, defined as active hydroxyl groups, were much larger than those detected by other conventional techniques. The concentration of the active hydroxyl groups on Co-Cr-Mo was significantly larger than those on cp-Ti and SS. Poly(ethylene glycol), PEG, is a biofunctional molecule that inhibits the adsorption of proteins. The immobilization of PEG to metal surfaces by electrodeposition or immersion is an important technique to biofunctionalize the metals. The amounts of the PEG layer immobilized on the metals were governed by the concentrations of the active hydroxyl groups on each surface oxide in the case of electrodeposition; it was governed by the relative permittivity of the surface oxide in the case of immersion. The estimation of active hydroxyl groups on the surface oxide film with the zinc-complex substitution technique is useful for the elucidation of reactions between metal substrates and immobilized molecules. [doi:10.2320/matertrans.MRA2007317]

(Received December 10, 2007; Accepted January 21, 2008; Published March 5, 2008)

Keywords: *titanium, poly(ethylene glycol), electrodeposition, active hydroxyl groups, X-ray photoelectron spectroscopy*

1. Introduction

When a metal is implanted into the human body, initial interactions occur between its surface and the biological environment. Therefore, the immediate reaction at this initial stage determines and defines tissue compatibility of metals. Conventional metals are covered by their native oxide films, which play an important role not only in corrosion resistance but also in compatibility. The surface oxide films are usually covered by hydroxyl groups and the mechanism underlying the hydroxylation of metal oxide has been investigated.[1)] The electric charge on the surface oxide film is another important factor governing tissue compatibility. The number of electric-charged sites on the surface corresponds to the number of hydroxyl groups that dissociate and form electric charges in aqueous solutions. These electric charges influence the adsorption manner of proteins, amino acids, and organic acids contained in body fluids. These adsorptions are followed by the adhesion of cells. Furthermore, the hydroxyl groups on the surface oxide film are relevant to interactions of the surface with ions, such as calcium and phosphate,[2)] as well as in respect to interactions of the surface with proteins, amino acids, and peptides, which generally contain domains of different electric charges.[3,4)] These initial reactions govern the resultant tissue compatibility of the metals.[5)] In other words, the hydroxyl groups on the surface oxide film influence the tissue compatibility of the metals.

These properties of the hydroxyl groups on the surface oxide film are not only relevant to its biocompatibility but may also influence the outcome of surface modification processes. Surface modification is the process whereby the surface properties change, leaving the bulk mechanical properties intact. In some surface modification techniques of the metals, the hydroxyl groups play an important role because they are the initiation sites for chemical reactions in the surface modification process.

The film on Ti consists of amorphous or low-crystalline and non-stoichiometric TiO_2 containing hydroxyl groups, and hydrate and/or adsorbed water.[6,7)] The surface oxide film of Ti polished in water contains not only Ti^{4+} but also Ti^{3+} and Ti^{2+};[8)] the surface oxide is not completely oxidized. In austenitic 316L stainless steel, the surface oxide film consists of Fe and Cr containing a small amount of Mo.[9)] According to another study, the surface oxide film on 316L steel after polishing consists of an oxide species of Fe, Cr, Ni, Mo, and Mn.[10)] The surface oxide film on a Co-Cr-Mo alloy consists of an oxide species of Co, Cr, and Mo.[11)] These surface oxide films contain a certain amount of hydroxyl groups. However, it is impossible to distinguish the active hydroxyl groups on the surface oxide film from those inside the surface oxide film as hydroxide with XPS alone. This means that the relationship between the concentrations of the hydroxyl groups on the surface oxide film and those inside the surface oxide film remains unclear. Another question is whether or not the concentrations of the hydroxyl groups on the surface oxide film are relevant to those of the hydroxyl groups inside the surface oxide film detected by XPS. The term "active hydroxyl groups" in this paper is defined as "hydroxyl groups located on the surface oxide film that easily react with some metal ions and form a metal complex," while the term "hydroxyl groups" usually refers to overall hydroxyl groups including inactive hydroxide inside the oxide film.

On the other hand, previous studies reported that poly-(ethylene glycol) terminated with amines at both terminals,

*1Graduate Student, Tokyo Medical and Dental University
*2Corresponding author, E-mail: tsutsumi.met@tmd.ac.jp

NH_2-PEG-NH_2, immobilized onto titanium oxide offered several biofunctions, such as the inhibition of protein adsorption and platelet adhesion.[12] The manner of NH_2-PEG-NH_2 immobilization was characterized by XPS and glow-discharge optical emission spectroscopy.[13] In the first layer of NH_2-PEG-NH_2 immobilized with electrodeposition, more terminated amines exist at the interface between the NH_2-PEG-NH_2 layer and titanium oxide and combine with titanium oxide as an NHO ionic bond formed between NH_3^+ and OH^-, while more amines randomly exist as NH_3^+ in the NH_2-PEG-NH_2 layer immobilized by immersion. These immobilization manners suggest that the immobilization of NH_2-PEG-NH_2 is directly relevant to the active hydroxyl groups on the surface oxide film of titanium. However, the relationship between the concentrations of the active hydroxyl groups on the metals and the amount of immobilized NH_2-PEG-NH_2 is unclear.

In this study, we compared the concentrations of the active hydroxyl groups located on titanium, an austenitic stainless steel, and Co-Cr-Mo alloy with those of the hydroxyl groups inside the surface oxide films. They were evaluated using XPS and a zinc-complex substitution technique. This study will enhance the understanding of the relationship between the active hydroxyl groups on these materials and the hydroxyl groups inside them. Another purpose of this study was to determine the predominant factors governing the immobilization of NH_2-PEG-NH_2 by electrodeposition or immersion.

2. Materials and Methods

2.1 Specimen preparation

The materials employed in this study were a commercially pure Ti with grade 2, cp-Ti, (Rare Metallic Co., Ltd., Japan), a type 316L austenitic stainless steel, SS, (Daido Steel Co., Ltd., Japan), and Co-Cr-Mo alloy, Co-Cr-Mo, (Daido Steel Co., Ltd., Japan). The chemical compositions of these materials are summarized in Tables 1–3. The Co-Cr-Mo was originally manufactured on the basis of a Co-28Cr-6Mo alloy (ISO 5832-4:1996). Rods of these materials were cut into disks with 8 mm in diameter and 2 mm in thickness. These disks were mirror-polished with SiC paper, 9 µm-diamond suspension, and 0.04 µm-colloidal silica suspension. The disks were cleaned from macroscopic contamination by ultrasonication in acetone for 0.9 ks, dried with a stream of nitrogen, and stored in a desiccator until the experiment.

Table 1 Chemical composition of a commercially pure Ti with grade 2 (mass%).

H	O	N	Fe	Ti
<0.0125	<0.25	<0.03	<0.05	Balance

Table 2 Chemical composition of a 316L stainless steel alloy (mass%).

C	Si	Mn	P	S
0.010	0.26	1.62	0.034	0.013
Ni	Cr	Mo	Fe	
12.07	16.62	2.10	Balance	

Table 3 Chemical composition of a Co-Cr-Mo alloy (mass%).

C	Si	Mn	P
0.082	<0.01	0.50	<0.003
S	Cu	Ni	Cr
0.001	<0.01	0.15	27.87
Mo	N	Fe	Co
6.14	0.002	0.11	Balance

2.2 Concentrations of hydroxyl groups

2.2.1 XPS analysis

XPS was performed with an electron spectrometer (SSX-100, Surface Science Instrument, USA). All binding energies given in this paper are relative to the Fermi level, and all spectra were excited with the monochromatized Al Kα line (1486.61 eV). The spectrometer was calibrated against Au $4f_{7/2}$ (binding energy, 84.07 eV) and Au $4f_{5/2}$ (87.74 eV) of pure gold and Cu $2p_{3/2}$ (932.53 eV), Cu $2p_{1/2}$ (952.35 eV), and the Cu Auger $L_3M_{4,5}M_{4,5}$ line (kinetic energy, 918.65 eV) of pure copper. The energy values were based on published data.[14] In order to estimate the photoelectron peak intensities, the background was subtracted from the measured spectrum according to Shirley's method.[15] An angle-resolved technique for XPS was applied to specimens at photoelectron take-off angles of 12°, 24°, 35°, 53°, and 90°, where the take-off angle is defined as the angle between the direction of the photoelectron path to the electron spectrometer and specimen surface. The composition and thickness of the surface oxide film were simultaneously calculated from data at the take-off angles of 35° according to previous studies.[16,17] Empirical data[18,19] and theoretically calculated data[20] of the relative photoionization cross-sections were used for the quantification. The relative photoionization cross-sections used in this study are summarized in Table 4.[16–20]

2.2.2 Zinc-complex substitution technique

The concentrations of active hydroxyl groups existing on metals were determined by the following methods.[21] An ammonium chloride solution (4.0 mol L^{-1} and 50 mL) was mixed with a zinc chloride (0.4 mol L^{-1} and 25 mL) solution, and the pH of the mixture was adjusted to 6.9 with 30% ammonium hydroxide. The volume of the mixture was adjusted to 100 mL with deionized water. Specimens were immersed in 30 mL of the resultant solution at ambient temperature for 0.3 ks. During immersion, one zinc complex

Table 4 Photoionization cross-sections of level j of element i relative to that of the O1s, σ_{ij}/σ_{O1s}.

Photoionization cross-section					
Level	Ti $2p_{3/2}$	Fe $2p_{3/2}$ (Metal)	Fe $2p_{3/2}$ (Oxide)	Cr $2p_{3/2}$	Mo $3d_{5/2}$
σ_{ij}/σ_{O1s}	1.28	2.46	1.45	1.71	3.46
Reference	18	16	16	16	19
Level	Ni $2p_{3/2}$ (Metal)	Ni $2p_{3/2}$ (Oxide)	Mn $2p_{3/2}$	Co $2p_{3/2}$ (Metal)	Co $2p_{3/2}$ (Oxide)
σ_{ij}/σ_{O1s}	2.3	7.47	3.15	4.5	3.9
Reference	17	18	20	17	17

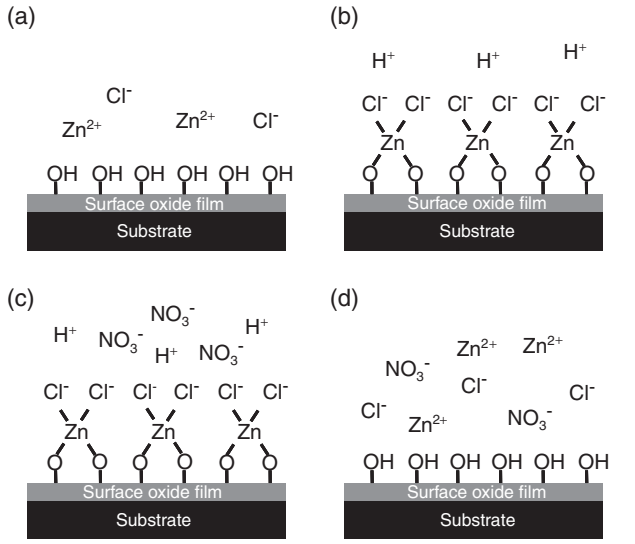

Fig. 1 Formation and release of the zinc complex by the reaction of active hydroxyl groups (OH) on the surface oxide film with a zinc chloride reagent.

was formed with two hydroxyl groups (Figs. 1(a) and (b)). The specimens were then immersed in 30 mL of deionized water twice to remove chemical species without adsorption and dried in a desiccator for 3.6 ks. After drying, the specimens were characterized using XPS to verify the zinc complex formed on the specimens. The specimens were then immersed in 40 mL of 2.5 mol L^{-1} nitric acid for 0.6 ks to release zinc ions into the nitric acid solution (Figs. 1(c) and (d)). The volume of the solution containing zinc ions was adjusted to 50 ml with nitric acid. The concentration of zinc ions, C_{Zn}, in the nitric acid solution was determined using an inductively coupled plasma atomic emission spectrometer (ICP-AES: PS-3000UV, Leeman Labs, Inc., Lowell, MA). The concentration of the zinc ions per unit surface area of each metal, N_{Zn}, was calculated according the following equation:

$$N_{Zn} = C_{Zn} V N_A / M_{Zn} S, \quad (1)$$

where V is the volume of nitric acid (50 mL), N_A is the Avogadro number (6.02×10^{23}), S is the surface area of the specimen, and M_{Zn} is the molecular weight of zinc (62.75). N_{Zn} is proportional to the concentrations of active hydroxyl radicals on the surface oxide film. In other words, twice N_{Zn} equals the number of active hydroxyl groups, $C_{active\text{-}OH}$. The method is described in detail elsewhere.[21,22] Each $C_{active\text{-}OH}$ values of SS and Co-Cr-Mo were normalized by that of cp-Ti, assuming that the surface roughness and reactivity of zinc ions are almost the same for each metal.

2.3 Immobilization of PEG terminated with amine

Both terminals of PEG were terminated with amines, NH_2-PEG-NH_2, (PEG1000 Diamine, NOF Corporation, Japan) as shown in Fig. 2. NH_2-PEG-NH_2 was dissolved in 0.3-mol L^{-1} NaCl solution at the concentrations of 2 mass%. In the solution, the -NH_2 terminals are pertially dissociated and positively charged as -NH_3^+. The pH of the NH_2-PEG-NH_2 solution was 11. The resultant solution was used as an electrolyte for electrodeposition at 310 K. Specimens were

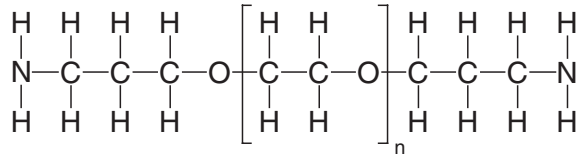

Fig. 2 Chemical structures of PEG terminated at both terminals with an amine, NH_2-PEG-NH_2.

fixed in a polytetrafluoroethylene holder that was insulated from the electrolyte in the exception of an open window (28.3 mm^2). The open circuit potential of specimens, OCP, against a saturated calomel electrode, SCE, before electrodeposition was measured. Thereafter, the cathodic potential was appplied from OCP with a constant sweep rate of -0.1 V s^{-1} and maintained at to -5.0 V_{SCE} for 0.3 ks. During cathodic polarization, NH_2-PEG-NH_2 migrated to the cathode (specimen), where it was immobilized. In addition, the solution without NaCl was used for immobilization by immersion. Specimens were immersed in the solution for 24 h. After electrodeposition and immersion, each specimen was rinsed in deionized water and dried with a stream of nitrogen (99.9%).

2.4 Thickness of the PEG layer

The thicknesses of the NH_2-PEG-NH_2 layer immobilized to the metals after electrodeposition or immersion were determined with an ellipsometer (DVA-36Ls, Mizojiri Optical Co., Ltd., Japan) in air. The light source was a He-Ne laser with a wavelength of 632.8 nm, and the incident angle to the surface of the specimen was 70°. The thickness was calculated using a refraction index, n, and an extinction coefficient, k, obtained from another metal surface without PEG layer: the n and k of cp-Ti were 2.39 and 3.07, those of SS were 2.49 and 4.19, and those of Co-Cr-Mo were 1.73 and 3.84, respectively.

2.5 Statistical analysis

A statistical comparison was made using the one-way factorial ANOVA including the interaction effect (two-tailed and $p \leq 0.05$) and post-hoc Tukey multiple comparison testing.

3. Results and Discussion

3.1 Hydroxyl groups detected with XPS

C was detected on all specimens before electrodeposition. From the C 1s spectra, it was concluded that none of the specimens contained carbonate because no peak was detected at an energy region of 289–290 eV, where carbonate should give a C 1s peak.[23] Therefore, C detected by XPS can be ascribed to so-called contaminant carbon. Apart from C, only Ti and O were detected from cp-Ti; Fe, Cr, Ni, Mo, Mn, and O were detected from SS; Co, Cr, Mo, and O were detected from Co-Cr-Mo. In addition to their oxide-state peaks, the metal-state peak of Ti 2p from cp-Ti, those of Fe 2p, Cr 2p, Ni 2p, Mo 3d, and Mn 2p from SS, and those of Co 2p, Cr 2p, and Mo 3d from Co-Cr-Mo derived from the substrates, were also detected. Therefore, the thicknesses of oxide layers of all specimens were smaller than the limit of detection depth

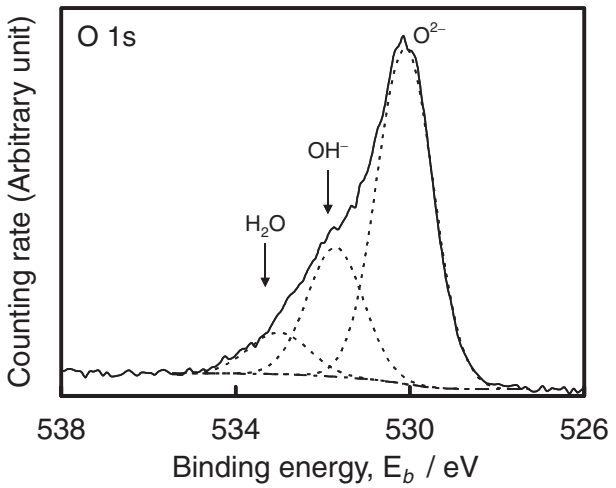

Fig. 3 Typical O 1s spectrum obtained from a metal surface and its deconvolution into O^{2-}, OH^-, and H_2O components.

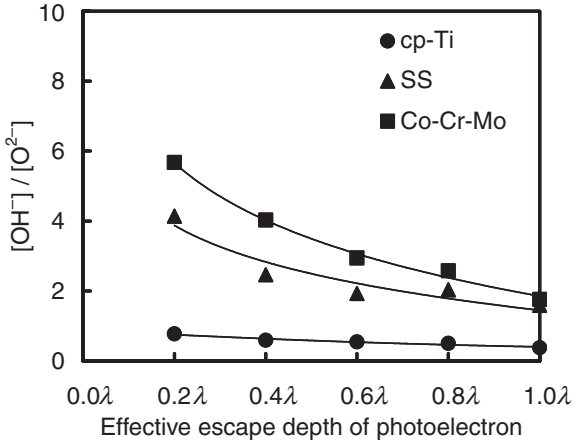

Fig. 4 Ratio of the proportion of the concentrations of OH^- to that of O^{2-} in a surface oxide film on metals plotted against the average effective escape depth of photoelectrons for angle-resolved XPS measurements. Lambda, λ, is the average escape depth of O 1s photoelectrons, and the effective escape depth is the escape depth times sin (take-off angle).

of XPS. In other words, whole hydroxyl groups on and inside the surface oxide film were detected.

The XPS spectrum of the O 1s electron binding energy region consists of at least three peaks originating from oxide, O^{2-}, hydroxyl groups, OH^-, and hydrate and/or adsorbed water, H_2O, as shown in Fig. 3. The $[OH^-]/[O^{2-}]$ ratio obtained by the angle-resolved technique is plotted versus the average escape depth of photoelectrons in Fig. 4. In the average effective escape depth of photoelectrons for angle-resolved XPS measurements, λ is the average mean free path of O 1s photoelectrons, and the effective escape depth is estimated as λ times sin (take-off-angle). The $[OH^-]/[O^{2-}]$ ratio of cp-Ti was much smaller than those of SS and Co-Cr-Mo; the ratio was the largest in this order: Co-Cr-Mo, SS, and cp-Ti. This order in the outer layer is the same as that in the inner layer as shown in Fig. 4. In addition, it can clearly be seen that the hydroxyl groups are distributed in the outer layer rather than in the inner layer in the surface oxide film because the ratio decreases with the increase in the effective escape depth of photoelectron, *i.e.*, with the depth of the

Table 5 Compositions and thickness, d, of surface oxide films of a commercially pure titanium, cp-Ti, a 316L stainless steel, SS, and a Co-Cr-Mo alloy, Co-Cr-Mo, determined by XPS.

Specimen	Concentration (mol%)										Thickness of film, d/nm
	Ti	Fe	Cr	Co	Ni	Mo	Mn	O^{2-}	OH^-	H_2O	
cp-Ti	29.1	—	—	—	—	—	—	38.2	20.6	12.1	3.7
SS	—	19.7	3.6	—	0.5	0.3	0.5	21.9	42.2	11.3	3.6
Co-Cr-Mo	—	—	10.0	11.0	—	1.1	—	17.0	50.0	10.9	2.5

oxide film. The concentration gradient in Co-Cr-Mo can be described as an enrichment of the hydroxyl groups in the outer layer.

Table 5 represents the compositions of the surface oxide film in cp-Ti, SS, and Co-Cr-Mo measured at a take-off angle of 35°.[24,25] The compositions shown in Table 5 were calculated without C, because the detected C was originated from so-called contaminant C. The hydroxyl groups in Co-Cr-Mo accounted for one half the composition of the surface oxide film. The table also contains the thickness of the surface oxide films. The thin surface oxide layer of Co-Cr-Mo emphasizes the enrichment of the hydroxyl groups in the outer layer. However, it is still unclear whether or not the concentrations of the hydroxyl groups detected under an ultrahigh vacuum influenced in the chemical reaction in solution environment.

3.2 Active hydroxyl groups determined with the zinc-complex substitution technique

The XPS spectrum of Zn $2p_{3/2}$ shown in Fig. 5 is deconvoluted to two peaks: one peak is a predominant peak at a binding energy of about 1022 eV originating form ZnO formed between Zn^{2+} and O^-; the other peak is originating from $Zn(OH)_2$ and/or $ZnCl_2$ at 1023 eV (the peak is usually shifted to a higher binding energy by bonding with hydroxyl groups or chlorine.[26] Therefore, zinc combined with oxygen and chlorine; the existence of zinc complexes with hydroxyl groups and chloride were confirmed with XPS. Figure 6

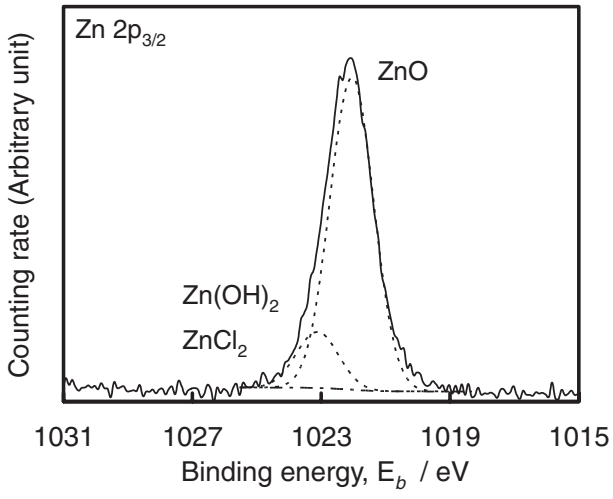

Fig. 5 Zn $2p_{3/2}$ spectrum obtained from titanium surface formed a zinc-complex and its deconvolution into ZnO and $Zn(OH)_2$, $ZnCl_2$ components.

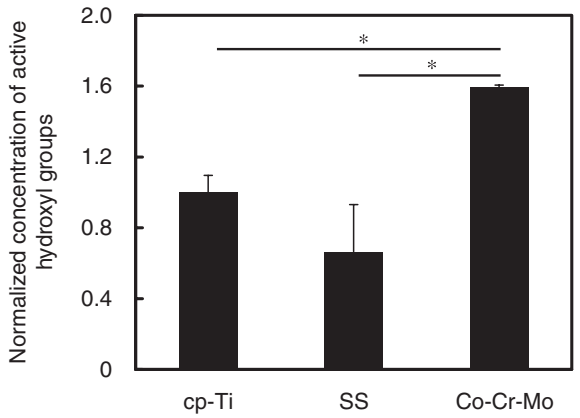

Fig. 6 Normalized concentration of active hydroxyl groups on a commercially pure titanium, cp-Ti, a 316L stainless steel, SS, and a cobalt-chromium-molybdenum alloy, Co-Cr-Mo, determined by using the zinc-complex substitution technique. Each $C_{\text{active-OH}}$ values of SS and Co-Cr-Mo were normalized by that of cp-Ti. The bars represent statistically significant differences ($p \leq 0.05$).

represents the normalized concentrations of active hydroxyl groups per unit area on the surface oxide film determined by the zinc-complex substitution technique. The $C_{\text{active-OH}}$ on cp-Ti was 285 nm^{-2} and this value was much larger than those (4.9–12.5 nm^{-2}) of deuterium exchange and crystallographic analysis[27,28] for the following reasons. It is possible that a zinc-complex multilayer network was formed onto the first zinc complex layer and the concentration of the zinc ion throughout the network was also detected by this technique. This multilayer will be formed by physical adsorption using chloride ions included in the zinc complex. As a result, $C_{\text{active-OH}}$ may be overestimated. However, the concentrations of zinc ions, including the zinc-complex network, are dependent on the concentrations of zinc ions in the first layer, *i.e.*, the concentration of the active hydroxyl groups on the surface oxide film. Another reason is the activation of the hydroxyl groups inside the surface oxide film. The hydroxyl groups inside the surface oxide film are consistently exchanged with those on the surface oxide film by the redox reaction in a solution. For this reason, the hydroxyl groups inside the surface oxide groups may be detected using this technique. However, $C_{\text{active-OH}}$ will hardly change under electrodeposition. In addition, a nanometer-scale surface roughness might contribute to the overestimation of the hydroxyl groups. In any case, this technique is suitable for relative evaluation rather than absolute one. Therefore, $C_{\text{active-OH}}$ was normalized by that of cp-Ti.

The $C_{\text{active-OH}}$ in Co-Cr-Mo were significantly larger than those in cp-Ti and SS ($p \leq 0.05$), but no significant difference was observed between cp-Ti and SS, as shown in Fig. 6. Surface hydroxyl groups easily form on the surface oxide film by the adsorption of water molecules.[29] This order was different from that in the results by XPS (Fig. 4). However, the concentrations of the hydroxyl groups on and inside the Co-Cr-Mo oxide film were the largest in both techniques. These results represent the activity of Co-Cr-Mo to form the hydroxyl groups on and inside the surface oxide film. The activity of Co-Cr-Mo is much larger than that of cp-Ti and SS. As a result, the surface of Co-Cr-Mo formed more hydroxyl groups than those of cp-Ti and SS.

The active hydroxyl groups located on the surface oxide film and the hydroxyl groups inside the surface oxide film are dependent on each other and easily interchangeable according to the redox reactions. Therefore, it is impossible to distinguish precisely between the two hydroxyl groups, while a rough distinction, such as the one made in this study, is useful for the estimation of the active hydroxyl groups located on the surface oxide film. The concentrations of the active hydroxyl groups determined by the chemical reaction in a solution were much larger than those detected under an ultrahigh vacuum. In addition, the active hydroxyl groups will be useful to evaluate the interfacial reaction in a solution rather than the hydroxyl groups inside the surface oxide film.

3.3 Predominant factors influencing the immobilization of PEG

The thicknesses of the NH_2-PEG-NH_2 layer immobilized with electrodeposition were the largest in Co-Cr-Mo, as shown Fig. 7. This relationship corresponds to that of the active hydroxyl groups on the surface oxide film. These results indicated that the active hydroxyl groups played an important role in immobilization by electrodeposition of NH_2-PEG-NH_2, while they did not in that by immersion. In case of immersion, the thickness of PEG on the SS oxide film was significantly larger than those on cp-Ti and Co-Cr-Mo in Fig. 7.

A point of zero charge (pzc) is generally believed to be relevant to the chemical and biological behavior of oxides or oxide-covered metal surfaces in contact with water or body fluids. The pzc of each material might affect the thickness of the NH_2-PEG-NH_2 layer in immobilization by immersion. The pzc values are obtained from weighted average values calculated with both the pzc of metal oxides shown in Table 6[30,31] and compositions of each surface oxide film determined using XPS (Table 5). The pzc values are listed in Table 7. The surfaces of cp-Ti and SS are negatively charged because the pzc values in cp-Ti and SS are much smaller than the pH of the NH_2-PEG-NH_2 solution, *i.e.*, pH 11. On the other hand, the pzc in Co-Cr-Mo is close to the pH of the

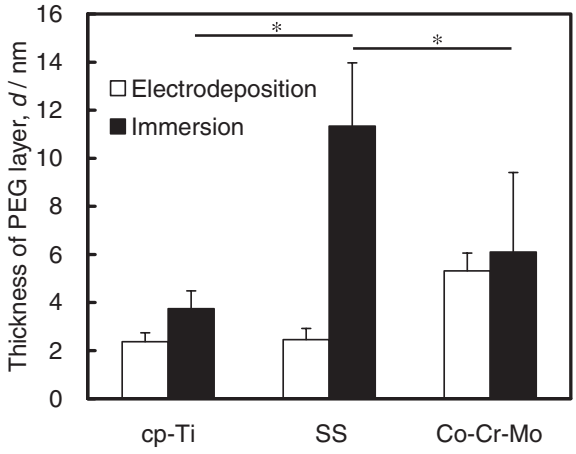

Fig. 7 Thickness of the NH_2-PEG-NH_2 layer on a commercially pure titanium, cp-Ti, a 316L stainless steel, SS, and a cobalt-chromium-molybdenum alloy, Co-Cr-Mo. The bars represent statistically significant differences ($p \leq 0.05$).

Table 6 Average values of point of the zero charges of oxides in a commercially pure titanium, cp-Ti, a 316L stainless steel, SS, and a cobalt-chromium-molybdenum alloy, Co-Cr-Mo.

Oxide (in each metal)	Average point of zero charge
TiO_2 (cp-Ti)	5.1
Fe_2O_3 (SS)	5.6
Cr_2O_3 (SS and Co-Cr-Mo)	7.1
Co_2O_3 (Co-Cr-Mo)	10.8

Table 7 Point of zero charge of a commercially pure titanium, cp-Ti, a 316L stainless steel, SS, and a Co-Cr-Mo alloy, Co-Cr-Mo, calculated from XPS data in Table 5.

Metal	Point of zero charge
cp-Ti	5.1
SS	5.8
Co-Cr-Mo	9.0

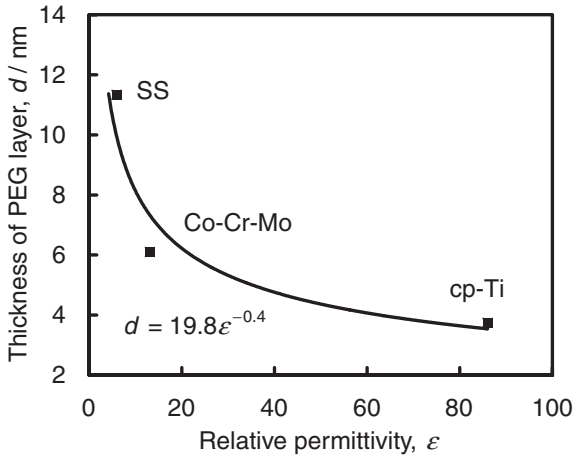

Fig. 8 Relationship between the relative permittivity and the thickness of the NH_2-PEG-NH_2 layer in a commercially pure titanium, cp-Ti, a 316L stainless steel, SS, and a cobalt-chromium-molybdenum alloy, Co-Cr-Mo.

NH_2-PEG-NH_2 solution. Therefore, there are few negatively charged sites on Co-Cr-Mo, and the reactivity between the electric-charged sites and the amine of NH_2-PEG-NH_2 in Co-Cr-Mo was smaller than those in cp-Ti and SS. As a result, the thickness of the NH_2-PEG-NH_2 layer in SS was greater than that in Co-Cr-Mo. However, the relationship between cp-Ti and SS still remains to be explained.

The electrostatic force of surface oxide on metals also might influence the adsorption of NH_2-PEG-NH_2 during immersion. Electrostatic force plays an important role for the adsorption manner of proteins to metal surfaces.[32] The electrostatic force is inversely proportional to the relative permittivity of the surface oxide covering each metal. Table 9 listed calculated values as weighted averages using both the relative permittivity of oxides (Table 8)[33] and compositions of each surface oxide film determined using XPS (Table 5). The relative permittivity was the smallest in this order: SS, Co-Cr-Mo, and cp-Ti, as shown in Table 9. The lower relative permittivity of a material is, the larger electrostatic force of a material to attract charged species being. In other words, a decrease in the thickness of PEG layer can be associated with an increase in the relative permittivity. As a result, the thicknesses of PEG layer immobilized on each specimens by immersion is inversely proportional to the relative permittivity of each oxide film (the correlation factor, R^2, is 0.91), as shown in Fig. 8. The order of the thickness of PEG immobilized by immersion was the largest in this order: SS, Co-Cr-Mo, and cp-Ti, which corresponded to that of the electrostatic force, *i.e.*, the reverse sequence of the relative permittivity. Therefore, the relative permittivity of surface oxides on the metals played an important role in immobilization by immersion.

The ratio of the reaction between the active hydroxyl groups on the surface oxide film and amines in NH_2-PEG-NH_2 is higher in electrodeposition than in immersion because the large external potential was applied. Therefore, the magnitude correlation of active hydroxyl groups corresponded to that of the thicknesses of the NH_2-PEG-NH_2 layer immobilized by electrodeposition. Subsequently, the thickness in 300-s electrodeposition was larger than that in 2-h immersion (previous study), and electrodeposition was more effective than immersion for the immobilization of PEG.[12]

Table 8 Relative permittivity of oxides in a commercially pure titanium, cp-Ti, a 316L stainless steel, SS, and a cobalt-chromium-molybdenum alloy, Co-Cr-Mo.

Oxide (in each metal)	Relative permittivity
TiO_2 (cp-Ti)	86.0
Fe_2O_3 (SS)	4.5
Cr_2O_3 (SS and Co-Cr-Mo)	13.3
CoO (Co-Cr-Mo)	12.9

Table 9 Relative permittivity of surface oxide films in a commercially pure titanium, cp-Ti, a 316L stainless steel, SS, and a cobalt-chromium-molybdenum alloy, Co-Cr-Mo.

Metal	Relative permittivity
cp-Ti	86.0
SS	5.9
Co-Cr-Mo	13.1

4. Conclusions

The concentrations of the hydroxyl groups located on and inside the surface oxide films of cp-Ti, SS, and Co-Cr-Mo were evaluated using XPS and the zinc-complex substitution technique. The concentrations of hydroxyl groups detected with the zinc-complex substitution technique were much larger than those calculated by other conventional techniques. The concentrations of the hydroxyl groups in Co-Cr-Mo were the largest in both techniques. Therefore, the surface activity of Co-Cr-Mo is possibly much larger than those of cp-Ti and SS. This estimation of the active hydroxyl groups on the surface oxide film with the zinc-complex substitution technique was useful for the reaction between the metal oxide and PEG. As a result, the relative permittivity of surface oxides was a predominant factor for the immobilization of PEG by immersion, while the concentrations of the active hydroxyl groups were the predominant factor in the immobilization by electrodeposition.

Acknowledgements

We are grateful to Prof. K. Asami, Prof. H. Kimura, and Mr. Ohtsu, Institute of Material Research, Tohoku University for their assistance with XPS. The study was performed under the inter-university cooperative research program of Laboratory for Advanced Materials, Institute of Materials Research, Tohoku University.

REFERENCES

1) H. Tamura, K. Mita, A. Tanaka and M. Ito: J. Colloid Interface Sci. **243** (2001) 202–207.
2) Y. Tanaka, E. Kobayashi, S. Hiromoto, K. Asami, H. Imai and T. Hanawa: J. Mater. Sci. Mater. Med. **18** (2007) 797–806.
3) J. A. Lori and T. Hanawa: Corros. Sci. **43** (2001) 21111–21120.
4) G. Iucci, M. Dettin, C. Battocchio, R. Gambaretto, C. Di Bello and G. Polzonetti: Mater. Sci. Eng. C (in press).
5) B. Kasemo and J. Lausmaa: CRC Crit. Rev. Biocompat. **2** (1986) 335–380.
6) E. L. Bullock, L. Patthey and S. G. Steinemann: Surf. Sci. **352** (1996) 504–510.
7) K. E. Healy and P. Ducheyne: Biomaterials **13** (1992) 553–561.
8) K. Asami, S. C. Chen, H. Habazaki and K. Hashimoto: Corros. Sci. **35** (1993) 43–49.
9) P. Brüesch, K. Müller, A. Atrens and H. Neff: Appl. Phys. A **38** (1985) 1–18.
10) T. Hanawa, S. Hiromoto, A. Yamamoto, D. Kuroda and K. Asami: Mater. Trans. **43** (2002) 3088–3092.
11) T. Hanawa, S. Hiromoto and K. Asami: Appl. Surf. Sci. **183** (2001) 68–75.
12) Y. Tanaka, H. Doi, Y. Iwasaki, S. Hiromoto, T. Yoneyama, K. Asami, H. Imai and T. Hanawa: Mater. Sci. Eng. C **27** (2007) 206–122.
13) Y. Tanaka, H. Doi, E. Kobayashi, T. Yoneyama and T. Hanawa: Mater. Trans. **48** (2007) 287–292.
14) K. Asami: J. Electron Spectrosc. **9** (1976) 469–478.
15) D. A. Shirley: Phys. Rev. B **5** (1972) 4709–4715.
16) K. Asami, K. Hashimoto and S. Shimodaira: Corros. Sci. **17** (1977) 713–723.
17) K. Asami and K. Hashimoto: Corros. Sci. **24** (1984) 83–97.
18) K. Asami, S. C. Chen, H. Habazaki, A. Kawashima and K. Hashimoto: Corros. Sci. **31** (1990) 727–732.
19) K. Asami and K. Hashimoto: Corros. Sci. **17** (1977) 559–570.
20) J. H. Scofield: J. Electron Spectrosc. **8** (1976) 129–137.
21) M. Imai and M. Nishio: Sumitomo-Kinzoku-giho **30** (1980) 72–77.
22) A. Kozawa: J. Electrochem. Soc. **106** (1959) 552–556.
23) J. S. Hammond, J. W. Holubka, J. E. de Vries and R. A. Dickie: Corros. Sci. **21** (1981) 239–253.
24) T. Hanawa, S. Hiromoto, A. Yamamoto, D. Kuroda and K. Asami: Mater. Trans. **43** (2002) 3088–3092.
25) T. Hanawa, S. Hiromoto and K. Asami: Appl. Surf. Sci. **183** (2001) 68–75.
26) D. Briggs and M. P. Seah: *Practical Surface Analysis 2nd Edt*, (John Willey & Sons, Chichester, 1990) Appendix 5.
27) H. Tamura and R. Furuichi: Bull. Jpn. Inst. Metal **27** (1988) 158–164.
28) E. McCafferty and J. P. Wightman: Sur. Interface Anal. **26** (1998) 549–564.
29) H. P. Boehm: Angew. Chem. **5** (1966) 533–544.
30) G. A. Parks: Chem. Rev. **65** (1965) 177–198.
31) D. M. Brunette, P. Tengvall, M. Textor and P. Thomsen: *Titanium in Medicine*, (Springer-Verlag, Berlin and Heidelberg, Germany, 2001) pp. 171–230.
32) J.-E. Sundgren, P. Bodö, B. Ivarsson and I. Lundström: J. Colloid Interface Sci., **113** (1986) 530–543.
33) D. R. Lide: *CRC Handbook of Chemistry and Physics 87th ed.*, (CRC Press, Boca Raton, Florida, 2006) pp. 1244–1252.